반도체디스플레이기술학회지 제20권 제3호(2021년 9월)
Journal of the Semiconductor & Display Technology, Vol. 20, No. 3. September 2021.

Semi-analytical Numerical Analysis of the Core-size and Electric-field Intensity Dependency of the Light Emission Wavelength of CdSe/ZnS Quantum Dots

Honyeon Lee[*,**†]

[*†]Department of Electronics & Information Engineering, Soonchunhyang University, Asan, Chungnam 336-745, Korea,
[**]Department of Electronic Materials and Devices Engineering, Soonchunhyang University, Asan, Chungnam 336-745, Korea

ABSTRACT

I performed a semi-analytical numerical analysis of the effects of core size and electric field intensity on the light emission wavelength of CdSe/ZnS quantum dots (QDs). The analysis used a quantum mechanical approach; I solved the Schrödinger equation describing the electron-hole pairs of QDs. The numerical solutions are described using a basis set composed of the eigenstates of the Schrödinger equation; they are thus equivalent to analytical solutions. This semi-analytical numerical method made it simple and reliable to evaluate the dependency of QD characteristics on the QD core size and electric field intensity. As the QD core diameter changed from 9.9 to 2.5 nm, the light emission wavelength of CdSe core-only QDs varied from 262.9 to 643.8 nm, and that of CdSe/ZnS core/shell QDs from 279.9 to 697.2 nm. On application of an electric field of 8×10^5 V/cm, the emission wavelengths of green-emitting CdSe and CdSe/ZnS QDs increased by 7.7 and 3.8 nm, respectively. This semi-analytical numerical analysis will aid the choice of QD size and material, and promote the development of improved QD light-emitting devices.

Key Words : Quantum Dots, Core Size, Electric Field Intensity, Emission Wavelength

1. Introduction

Quantum dots (QDs) are expected to replace the organic light-emitting diodes (OLEDs) currently extensively used in displays. The QD emission wavelength can be readily changed by varying QD size and the emission spectra are sharp[1]. Thus, QDs will replace OLED[2] and liquid crystal (LC) displays[3]. Even now, large televisions using QD films as color-converting layers are being produced; these devices exploit QD photoluminescence[4,5]. Quantum-dot light-emitting diode (QDLED) technology exploiting QD electro-luminescence is being actively developed by many research groups[6–10]; however a few issues must be addressed prior to widespread commercialization, including QDLED lifetime [11,12] and efficiency[13,14]. The light emission spectra of QDs differ from those of bulk materials because of quantum confinement effects. Different primary colors can be obtained from QDs made of the same material by varying the QD size. Thus, fabrication is much simpler than that of OLEDs, which require different materials for generating different colors.

The quantum-confined Stark effect (QCSE) is readily observed in the electroluminescence spectra of QDs[15–17]. The QCSE causes QD spectral shifts depending on the driving voltage. Hence, QDLEDs must be carefully driven to obtain the desired colors. Detailed studies on the dependency of emission spectra on QD size and driving conditions are required to establish a reliable QDLED technology. Numerical approaches can be effective. Emission wavelength variation by QD size and the applied electric field should be examined before designing and fabricating a QDLED device.

[†]E-mail: hnlee@sch.ac.kr

This requires the solving of a Schrödinger equation that considers the internal potential QD profile, and the Coulomb interaction between the electron and hole that constitute an exciton. Although differential equation-solving methods based on the finite difference method[18] or finite element method[19] can be used to this end, an analytical method using the basis set of a single-particle Hamiltonian and the perturbation caused by the electron/hole interaction is more appropriate to understand QD characteristics. However, it is difficult and inefficient to obtain analytical solutions of QD emission behaviors for QDs of various sizes exposed to different electric fields. Here, I adopt a semi-analytical approach to overcome this difficulty, and designed a numerical method imitating an analytical one[20]. The numerical method was used to evaluate quantum mechanical properties. It is based on solving the single-particle Schrödinger equation, with consideration of the perturbation terms associated with electron/hole interaction and the potential profile. The numerical method is relatively undemanding in terms of calculations, so the dependency of emission wavelength on QD size and electric field intensity was calculated using only a personal computer.

2. Methods

To examine QD properties, the Schrödinger quantum mechanical equation for an electron/hole pair was solved numerically. The equation considered the kinetic energy terms, potential energy terms associated with the conduction and valence band profiles of the QD core and shell, and Coulomb energy terms caused by interaction between the electron and hole that constitute an exciton. The Hamiltonian $\hat{\mathcal{H}}$ is the sum of the electron kinetic energy $\hat{T}_e$, the hole kinetic energy $\hat{T}_h$, the electron potential energy $\hat{V}_e$, the hole potential energy $\hat{V}_h$, and the Coulomb interaction energy $\hat{\mathcal{H}}_{int}$, calculated as follows:

$$\left.\begin{aligned}
&\hat{\mathcal{H}} = \hat{T}_e + \hat{T}_h + \hat{V}_e + \hat{V}_h + \hat{\mathcal{H}}_{int},\\
&\hat{T}_e(\vec{r_e}) = -\frac{\hbar^2}{2m_e^*}\nabla_e^2,\\
&\hat{T}_h(\vec{r_h}) = -\frac{\hbar^2}{2m_h^*}\nabla_h^2,\\
&\hat{\mathcal{H}}_{int}(|\vec{r_e}-\vec{r_h}|) = -\frac{1}{4\pi\epsilon}\frac{e^2}{|\vec{r_e}-\vec{r_h}|}
\end{aligned}\right\} \quad (1)$$

where m_e^*, m_h^*, ∇_e^2, ∇_h^2, $\vec{r_e}$, $\vec{r_h}$, ϵ, and e are the electron effective mass, hole effective mass, Laplacian operator of an electron, Laplacian operator of a hole, electron position vector, hole position vector, permittivity, and elementary charge, respectively.

For efficient calculation, the system was approximated using one-dimensional equations, as follows:

$$\left.\begin{aligned}
&\hat{\mathcal{H}}_{1D} = \hat{T}_{e1D} + \hat{T}_{h1D} + \hat{V}_{e1D} + \hat{V}_{h1D} + \hat{\mathcal{H}}_{int1D},\\
&\hat{T}_{e1D}(x_e) = -\frac{\hbar^2}{2m_e^*}\frac{\partial^2}{\partial x_e^2},\\
&\hat{T}_{h1D}(x_h) = -\frac{\hbar^2}{2m_h^*}\frac{\partial^2}{\partial x_h^2},\\
&\hat{\mathcal{H}}_{int1D} = -\frac{1}{3}\frac{1}{4\pi\epsilon}\frac{e^2}{\sqrt{3}|x_e-x_h|}
\end{aligned}\right\} \quad (2)$$

where $\hat{\mathcal{H}}_{1D}$, $\hat{T}_{e1D}$, $\hat{T}_{h1D}$, $\hat{V}_{e1D}$, $\hat{V}_{h1D}$, $\hat{\mathcal{H}}_{int1D}$, x_e, and x_h are the Hamiltonian, electron kinetic energy, hole kinetic energy, electron potential energy, hole potential energy, Coulomb interaction energy, electron position, and hole position in one dimension, respectively. The electron-hole distance is underestimated when the one-dimensional distance $|x_e - x_h|$ is used to calculate the Coulomb interaction energy term. To compensate for this, $\sqrt{3}|x_e - x_h|$ served as the electron-hole distance in the one-dimensional equation, given that $|\vec{r_e} - \vec{r_h}| = \sqrt{3}|x_e - x_h|$ for the symmetrical case of $|x_e - x_h| = |y_e - y_h| = |z_e - z_h|$. Hence, the electron-hole distance $\sqrt{3}|x_e - x_h|$ of Eq. (2) corresponds to the $|\vec{r_e} - \vec{r_h}|$ of Eq. (1). Therefore $-1/4\pi\epsilon \cdot e^2/\sqrt{3}|x_e - x_h|$ corresponds to the three-dimensional Coulomb interaction energy. Given this, a modification factor of $1/3$ was applied to the $\hat{\mathcal{H}}_{int1D}$ term to yield the Coulomb interaction energy in one dimension.

The basis set of the system consisted of the single-particle basis sets for an electron and a hole. For numerical calculation, the number of bases was restricted to a number n_{max} that could be handled by a personal computer. A momentum basis set was defined by reference to the kinetic energy operator for a single particle and the infinite well boundary condition. The n_{max} bases were selected from the lowest energy state in increasing energy order. The electron and hole system basis set was constructed using the tensor product of the single-particle basis sets, as follows:

$$|n,\tilde{n}\rangle = |n\rangle\otimes|\tilde{n}\rangle, for\ n,\tilde{n} \in \{1,2,3,\cdots,n_{max}\} \quad (3)$$

where $|n\rangle$ and $|\tilde{n}\rangle$ are the bases of an electron and a hole in infinite wells, respectively. In addition to the momentum basis set described above, a position basis set was defined to

handle the potential energy and Coulomb interaction energy terms. Equally spaced n_{max} points in the potential well were used to create this basis. The basis set was defined as follows:

$$|j\rangle = \sqrt{\Delta}\sum_{n=1}^{n_{max}} \phi_n(x_j)|n\rangle \text{ for } j \in \{1, 2, \cdots, n_{max}\} \quad (4)$$

In the equation above, Δ is the spacing between the equally spaced n_{max} points and $\phi_n(x)$ is the spatial wavefunction at position x (defined as $\langle x|n\rangle$, where $|x\rangle$ is the Dirac position basis). The electron and hole system basis sets were constructed using the tensor product of the single particle basis sets, as follows:

$$|j, \tilde{j}\rangle = |j\rangle \otimes |\tilde{j}\rangle, \text{for } j, \tilde{j} \in \{1,2,3, \cdots, n_{max}\} \quad (5)$$

where $|j\rangle$ and $|\tilde{j}\rangle$ are the single electron and single hole position bases, respectively.

The kinetic energy terms $\hat{T}_{e1D}$ and $\hat{T}_{h1D}$ represented by the momentum basis set are $\sum_{n=1}^{n_{max}} T_{e1D,n}|n\rangle\langle n|$ and $\sum_{\tilde{n}=1}^{n_{max}} T_{h1D,\tilde{n}}|\tilde{n}\rangle\langle\tilde{n}|$, respectively. $T_{e1D,n}$ and $T_{h1D,\tilde{n}}$ are $\left\langle n\left|\left(-\frac{\hbar^2}{2m_e^*}\frac{\partial^2}{\partial x_e^2}\right)\right|n\right\rangle$ and $\left\langle \tilde{n}\left|\left(-\frac{\hbar^2}{2m_h^*}\frac{\partial^2}{\partial x_h^2}\right)\right|\tilde{n}\right\rangle$, respectively. The momentum basis representation was transformed into a position basis representation using a discrete Fourier transform. Then, the matrix representation of the kinetic energy terms $\hat{T}_{e1D} + \hat{T}_{h1D}$ was obtained using the tensor products, as follows:

$$\left(\sum_{j_1=1}^{n_{max}}\sum_{j_2=1}^{n_{max}} \tilde{T}_{e1D,j_1j_2}|j_1\rangle\langle j_2|\right)\otimes I_2 + I_1\otimes\left(\sum_{\tilde{j}_1=1}^{n_{max}}\sum_{\tilde{j}_2=1}^{n_{max}} \tilde{T}_{h1D,\tilde{j}_1\tilde{j}_2}|\tilde{j}_1\rangle\langle\tilde{j}_2|\right), \quad (6)$$

where $\tilde{T}_{e1D,j_1j_2}$ and $\tilde{T}_{h1D,\tilde{j}_1\tilde{j}_2}$ are the position-basis matrix elements transformed from the momentum-basis matrix elements by the discrete Fourier transform, and I_1 and I_2 are the identity matrices. Using the position basis set, the matrix representation of the potential energy terms, $\hat{V}_{e1D} + \hat{V}_{h1D}$, is obtained as follows:

$$\left(\sum_{j=1}^{n_{max}} V_{e1D,j}|j\rangle\langle j|\right)\otimes I_2 + I_1\otimes\left(\sum_{\tilde{j}=1}^{n_{max}} V_{h1D,\tilde{j}}|\tilde{j}\rangle\langle\tilde{j}|\right), \quad (7)$$

where $V_{e1D,j}$ and $V_{h1D,\tilde{j}}$ are $\langle j|\hat{V}_{e1D}|j\rangle$ and $\langle\tilde{j}|\hat{V}_{h1D}|\tilde{j}\rangle$, respectively and I_1 and I_2 are the identity matrices. The matrix representation of the Coulomb interaction term, $\hat{\mathcal{H}}_{int1D}$, is written in the position basis, as follows:

$$\sum_{j=1}^{n_{max}}\sum_{\tilde{j}=1}^{n_{max}} V_{int1D,j\tilde{j}}|j,\tilde{j}\rangle\langle j,\tilde{j}|, \quad (8)$$

where $V_{int1D,j\tilde{j}}$ is $\langle j,\tilde{j}|\hat{\mathcal{H}}_{int1D}|j,\tilde{j}\rangle$. The Coulomb interaction energy term exhibits a singularity when the electron and hole are in the same position ($x_e = x_h$); a modified relation was used to avoid this singularity. The distance in one dimension, $|x_e - x_h|$, was replaced with a fixed value, δ, when the electron and hole approached each other within δ. The value of δ was set to 0.5 nm, given the distance between the lattice points of the QD materials evaluated in this work.

The representation of the total Hamiltonian matrix $(\hat{\mathcal{H}}_{1D})$ in the position basis was obtained by adding the kinetic, potential, and Coulomb interaction energy terms described above. Wolfram Mathematica [21] was used to perform the matrix operations and Fourier transform, and to calculate the eigenvalues and eigenstates of the $\hat{\mathcal{H}}_{1D}$. The total energies for three-dimensional QDs were estimated by adding the one-dimensional total energies in the x, y, and z directions.

3. Results and Discussion

The dependency of the emitted light wavelength on QD size was examined for core-only and core/shell QDs. The core-only QD was modeled as a one-dimensional infinite potential well, and the core/shell QD as a one-dimensional infinite potential well with a stepped potential profile (Figure 1). The core diameter and shell thickness, t_{shell}, of the one-dimensional infinite potential wells were set to $\sqrt[3]{\pi/6}\, d_{core}$ and $\sqrt[3]{\pi/6}\, t_{shell}$, respectively. The weighting factor $\sqrt[3]{\pi/6}$ was extracted by comparing the volume of the cube-shaped QD explored in this work to that of the spherical QD. The core material was CdSe and the shell material was ZnS [22,23]. The bandgap energy of the CdSe core, E_g, was 1.74 eV. The conduction band barrier, ΔE_C, and valence band barrier, ΔE_V, at the core/shell interface were 1.27 eV and 0.6 eV[24], respectively. Effective mass approximations were used for modeling; the effective masses of the electron and hole were set to 0.12- and 0.45-fold the electron rest mass, given the properties of the CdSe core material[25]. For efficient calculation, the same effective mass values were used for the core and shell of the QDs. When an electric field was applied, it was assumed to affect the x-direction only. Thus, the total energies of three-dimensional QDs with an applied electric field were estimated by adding two one-dimensional total energies (in the y and z directions) without applied electric fields and one-dimensional total energy (in

the x direction) with such a field. The total energies of three-dimensional QDs without an applied electric field were three times the total energy of a one-dimensional total energy without a field.

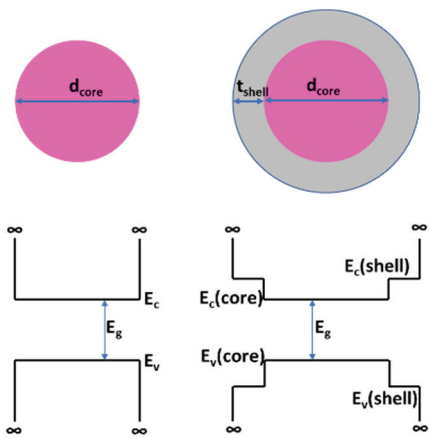

Fig. 1. Schematics of a core-only QD and potential profile model (left), and of a core/shell QD and potential profile model (right).

The band gap energy and the light emission wavelength are shown in Fig. 2 as functions of the QD diameter, d_{core},. For the core/shell QDs, the t_{shell} was 2.5 nm. The QD core diameter was varied from 2.5 to 9.9 nm. The QD band gap energy was estimated by adding the electron and hole ground state energies to the CdSe bulk band gap energy. Even for the largest-diameter (9.9 nm) d_{core}, the band gap energy increased considerably. For core-only QDs, the band gap energy and light emission wavelength varied from 1.93 eV and 643.8 nm for the 9.9-nm d_{core} to 4.72 eV and 262.9 nm, respectively, for the 2.5-nm d_{core}. For core/shell QDs, the band gap energy and light emission wavelength varied from 1.78 eV and 697.2 nm for the 9.9-nm d_{core} to 4.43 eV and 279.9 nm, respectively, for the 2.5-nm d_{core}. Hence, the emission color changed from red to ultraviolet as the core diameter changed from 9.9 to 2.5 nm. This smaller band gap energy of the core/shell QDs (compared to core-only QDs) is explained by the fact that the shell region contributes to wavefunction spreading in the core/shell QDs, thus alleviating the quantum confinement effects.

The effects of an applied electric field were estimated for core-only and core/shell QDs (Fig. 3). The core diameters of the core-only and core/shell QDs were 5.0 and 3.7 nm,

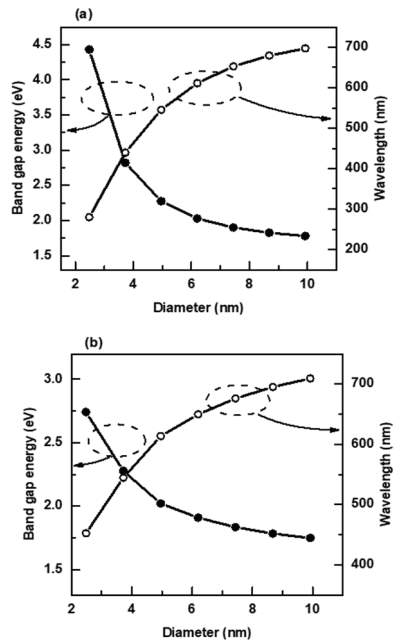

Fig. 2. Band gap energy and light emission wavelength as functions of the diameter of (a) core-only QDs and (b) core/shell QDs.

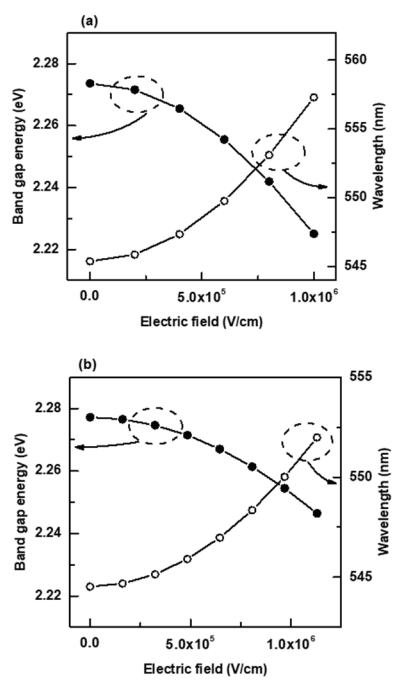

Fig. 3. Band gap energy and light emission wavelength as functions of the applied electric field intensity of (a) core-only QDs and (b) core/shell QDs.

respectively. These core diameters are the same as those of green-emitting QDs in the absence of an applied field; both emission wavelengths were about 545 nm. As shown in Fig. 3, the band gap energy decreases, and the emission wavelength increases, as the electric field increases. With an applied electric field of 8.0×10^5 V/cm, the emission wavelength shifted by 7.7 nm for the core-only QD and by 3.8 nm for the core/shell QD. Hence, the emission color can be controlled by application of an electric field. The QCSE explains the color shifts.

The spatial wavefunction distributions are shown in Fig. 4. Fig. 4(a) and (c) show the ground state wavefunction distributions of the core-only and core/shell QDs in the absence of an applied electric field, respectively, as functions of the electron and hole positions. Fig. 4(b) and (d) show the ground state wavefunction distributions of the core-only and core/shell QDs under an applied electric field of 8×10^5 V/cm, as functions of the electron and hole positions. Only the core regions are shown; the shell regions are excluded. When there is no electric field, the electron and hole gather in the center. When an electric field is applied, the wavefunction distributions of the electron and hole move in opposite directions to the core edges. However, the electron movement induced by an applied electric field is smaller than the hole movement. The electron and hole separate by moving in opposite directions toward the core edges when an electric field is applied. However, the Coulomb attraction between the electron and hole prohibits full separation. The electron effective mass is lighter than the hole effective mass; it is easier for the electron to be pulled toward the hole by Coulomb interaction than it is to pull the hole toward the electron. Hence, electron movement toward the core edge is limited.

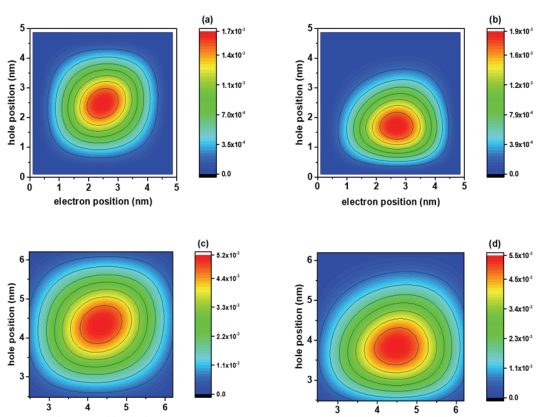

Fig. 4. Spatial wavefunction distribution of a core-only QD (a) without an applied electric field and (b) with an applied electric field, and of a core/shell QD (c) without an applied electric field and (d) with an applied electric field.

4. Conclusions

I designed a simple QD model amenable to effective numerical analysis. I studied the effects of core size and applied electric field intensity on the emission wavelength. The model and analysis were based on a quantum mechanical approach; I solved a Schrödinger equation that included kinetic, potential, and Coulomb interaction energies. The numerically obtained solutions were described using a basis set composed of the eigenstates of the quantum mechanical Schrödinger equation. Hence, the results of our numerical analysis are equivalent to analytical solutions, so the results are easy to understand and unlikely to be misinterpreted. By applying the semi-analytical numerical method to an electron/hole pair in a QD, the dependency of the QD characteristics on QD core size and electric field intensity can be examined in a simple and reliable manner.

Green emissions from core-only CdSe QDs and core/shell QDs with diameters of 5.0 and 3.7-nm, respectively, were confirmed; these core diameters accord with those of previous reports [26,27]. Hence, my modeling/solving method allows simple and reliable design of QD structures and aids in the choice of QD material. I found that the light emission wavelength was affected by the applied electric field intensity. Hence, the emission wavelengths of adjustable QDLEDs can be varied by controlling the intensity. My modeling/solving methods will aid the design and development of emission wavelength-adjustable QDLEDs. I am currently modeling emission color-controllable QDLEDs; in the near future, I plan to report an improved modeling and numerical analysis method, and experimental data on emission color-controllable QDLEDs.

Acknowledgements

This work was funded by BK21 FOUR (Fostering Outstanding Universities for Research) (No.: 5199991614 564) and by the Soonchunhyang University Research Fund.

References

1. P.O. Anikeeva, J.E. Halpert, M.G. Bawendi, V. Bulović, “Quantum Dot Light-Emitting Devices with Electroluminescence Tunable over the Entire Visible Spectrum”, Nano Lett., Vol. 9, pp. 2532-2536, 2009.
2. S.-J. Zou, Y. Shen, F.-M. Xie, J.-D. Chen, Y.-Q. Li, J.-X. Tang, “Recent advances in organic light-emitting diodes: toward smart lighting and displays”, Mater. Chem. Front., Vol. 4. pp. 788-820, 2020.
3. H.-W. Chen, J.-H. Lee, B.-Y. Lin, S. Chen, S.-T. Wu, “Liquid crystal display and organic light-emitting diode display: present status and future perspectives”, Light Sci. Appl., Vol. 7, 17168, 2018.
4. E. Lee, C.K. Wang, C. Hotz, J. Hartlove, J. Yurek, H. Daniels, Z. Luo, and D. Zehnder, ““Greener” Quantum-Dot Enabled LCDs with BT.2020 Color Gamut”, in: SID Symp. Dig. Tech. Pap., Wiley, pp. 549-551, 2016
5. J. Chen, V. Hardev, and J. Yurek, “Quantum-Dot Displays: Giving LCDs a Competitive Edge through Color”, Inf. Disp., Vol. 29, pp. 12-17, 2013.
6. Y. Shirasaki, G.J. Supran, M.G. Bawendi, and V. Bulović, “Emergence of colloidal quantum-dot light-emitting technologies”, Nat. Photonics, Vol. 7, pp. 13-23, 2013.
7. M.K. Choi, J. Yang, T. Hyeon, and D.-H. Kim, “Flexible quantum dot light-emitting diodes for next-generation displays”, Npj Flex. Electron., Vol. 2, 10, 2018.
8. W. Mei, Z. Zhang, A. Zhang, D. Li, X. Zhang, H. Wang, Z. Chen, Y. Li, X. Li, and X. Xu, “High-resolution, full-color quantum dot light-emitting diode display fabricated via photolithography approach”, Nano Res., Vol. 13, pp. 2485-2491, 2020.
9. X. Dai, Y. Deng, X. Peng, and Y. Jin, “Quantum-Dot Light-Emitting Diodes for Large-Area Displays: Towards the Dawn of Commercialization”, Adv. Mater., Vol. 29, 1607022, 2017.
10. Q. Yuan, T. Wang, P. Yu, H. Zhang, H. Zhang, W. Ji, “A review on the electroluminescence properties of quantum-dot light-emitting diodes”, Org. Electron., Vol. 90, 106086, 2021.
11. H. Moon, C. Lee, W. Lee, J. Kim, and H. Chae, “Stability of Quantum Dots, Quantum Dot Films, and Quantum Dot Light-Emitting Diodes for Display Applications”, Adv. Mater., Vol. 31, 1804294, 2019.
12. S.C. Hsu, L.A. Ke, H.C. Lin, T.M. Chen, H.Y. Lin, Y.Z. Chen, Y.L. Chueh, H.C. Kuo, C.C. Lin, “Fabrication of a Highly Stable White Light-Emitting Diode with Multiple-Layer Colloidal Quantum Dots”, IEEE J. Sel. Top. Quantum Electron., Vol. 23, 2000409, 2017.
13. Y. Sun, Y. Jiang, X.W. Sun, S. Zhang, and S. Chen, “Beyond OLED: Efficient Quantum Dot Light-Emitting Diodes for Display and Lighting Application”, Chem. Rec., Vol. 19, pp. 1729-1752, 2019.
14. M. Lu, J. Guo, S. Sun, P. Lu, X. Zhang, Z. Shi, W.W. Yu, Y. Zhang, “Surface ligand engineering-assisted CsPbI3 quantum dots enable bright and efficient red light-emitting diodes with a top-emitting structure”, Chem. Eng. J., Vol. 404, 126563, 2021.
15. X. Han, G. Zhang, B. Li, C. Yang, W. Guo, X. Bai, P. Huang, R. Chen, C. Qin, J. Hu, Y. Ma, H. Zhong, L. Xiao, and S. Jia, “Blinking Mechanisms and Intrinsic Quantum-Confined Stark Effect in Single Methylammonium Lead Bromide Perovskite Quantum Dots”, Small, Vol. 16, 2005435, 2020.
16. L. Zhang, B. Lv, H. Yang, R. Xu, X. Wang, M. Xiao, Y. Cui, and J. Zhang, “Quantum-confined stark effect in the ensemble of phase-pure CdSe/CdS quantum dots”, Nanoscale, Vol. 11, pp. 12619-12625, 2019.
17. Z.B. Wang, J.Y. Zhang, Y.P. Cui, and Y.H. Ye, “Effect of electrical field on colloidal CdSe/ZnS quantum dots”, Chinese Phys. Lett., Vol. 25, pp. 4435-4438, 2008.
18. T.E. Simos, and P.S. Williams, “A finite-difference method for the numerical solution of the Schrödinger equation”, J. Comput. Appl. Math., Vol. 79, pp. 189-205, 1997.
19. N. Sato, and S. Iwata, “Application of finite-element method to the two-dimensional Schrödinger equation”, J. Comput. Chem., Vol. 9, pp. 222-231, 1988.
20. R. Schmied, Using Mathematica for Quantum Mechanics, 1st ed., Springer Singapore, Singapore, 2020.
21. I. Wolfram Research, Mathematica, (2016). https://www.wolfram.com/mathematica/.
22. B.O. Dabbousi, J. Rodriguez-Viejo, F. V. Mikulec, J.R. Heine, H. Mattoussi, R. Ober, K.F. Jensen, and M.G. Bawendi, “(CdSe)ZnS core-shell quantum dots: Synthesis and characterization of a size series of highly luminescent nanocrystallites”, J. Phys. Chem. B., Vol. 101, pp. 9463-9475, 1997.
23. D.J. Kim, and H.N. Lee, “Improving the charge balance and performance of CdSe/ZnS quantum-dot light-emitting diodes with a sputtered zinc-tin-oxide electron-transport layer and a thermally evaporated tungsten-oxide charge-restricting layer”, Jpn. J. Appl. Phys., Vol. 58, 106502, 2019.
24. A. Samanta, Z. Deng, and Y. Liu, “Aqueous synthesis

of glutathione-capped CdTe/CdS/ZnS and CdTe/CdSe/ZnS core/shell/shell nanocrystal heterostructures", Langmuir, Vol. 28, pp. 8205-8215, 2012.
25. E.J. Tyrrell, and J.M. Smith, "Effective mass modeling of excitons in type-II quantum dot heterostructures", Phys. Rev. B - Condens. Matter Mater. Phys., Vol. 84, 165238, 2011.
26. S. Baskoutas, and A.F. Terzis, "Size-dependent band gap of colloidal quantum dots", J. Appl. Phys., Vol. 99, 013708, 2006.
27. E.O. Chukwuocha, M.C. Onyeaju, and T.S.T. Harry, "Theoretical Studies on the Effect of Confinement on Quantum Dots Using the Brus Equation", World J. Condens. Matter Phys., Vol. 02, pp. 96-100, 2012.

접수일: 2021년 8월 8일, 심사일: 2021년 9월 11일,
게재확정일: 2021년 9월 16일